동다짐시 동적 거동 계측
Dynamic measurement during Dynamic Compaction

나영묵[1], Yung-Mook Na,

[1] 현대건설(주) 창이매립공사 과장, Senior Geotechnical Engineer, Reclamation at Changi East
Hyundai Engineering & Construction Co., Ltd.(HDEC)

SYNOPSIS : 현재 국내외에서 해안가에 수심이 낮은 지역을 중심으로 대규모 매립공사를 수행하여 주택단지, 항만시설, 공업단지 및 공항부지 등으로 사용하고 있다. 매립재를 양질의 모래로 사용하는 경우 매립방법에 따라 매립토의 조밀정도는 다르나 어떠한 경우든 상당히 느슨하거나 중간정도 느슨한 상태로 존재한다. 이러한 느슨한 사질토는 지진 시 액상화 현상에 민감하고, 낮은 지지력 및 큰 즉시침하를 야기시킨다. 따라서 매립된 느슨한 사질토는 향후 시설될 구조물의 중요도에 따라 개량할 필요가 있다. 본 현장의 준설 매립된 사질토의 지반 개량에 적용된 동다짐의 시험시공중 pounder에 accelerometer를 설치하고 적외선 beam을 이용, 충격시의 pounder의 deceleration과 impact velocity를 측정하였다. 여기에서는 이들 실측치를 근거로 중량물체(pounder)의 동적 거동 및 충격시 과잉간극수압 변화를 살펴보았다.

KEYWORDS : Dynamic compaction, Dynamic measurement, Acceleration, Impact velocity

1. INTRODUCTION

Limited land space in many countries in Southeast and East Asia required land to be reclaimed from the sea. Reclaimed lands, which are particularly formed by hydraulic sandfill, are usually in need of soil improvement, in order to meet foundation requirement with respect to bearing capacity or settlement. For instance, airport runways are sensitive to dynamic loading and differential settlements. There are several methods that have been found to be effective in improving the mechanical properties of loose sand deposits. One of the commonly adopted methods is dynamic compaction. Dynamic compaction operates on the principle that the impact of sufficient magnitude of energy may rearrange the sand particles into a denser state.

Soil densification by dynamic compaction requires systematic application of high energy by a heavy pounder onto the ground surface in order to densify the underlying soil. The high dynamic energy applied to the surface of the soil deposit must be transmitted to the soil layers at depth. This is achieved by the propagation of different wave types such as shear wave and compression waves, which force the soil particles into a denser state. The pounders are usually square or circular in shape and made of steel or concrete. Their weights normally range from 5 to 40 tons

and drop heights of up to 25 m have been used frequently. Due to the lack of a proper understanding of the mechanism of dynamic compaction, most dynamic compaction projects are carried out by specialist contractors in aid of the trial compaction. Presently, a rational or well-established design procedure is not available. It is believed that a proper measurement of dynamic response on the pounder during dynamic compaction is useful for a better understanding of the dynamic compaction mechanism.

This paper presents a field measuring method for dynamic compaction. The tests were carried out at Changi East 1B reclamation site in Singapore. The purpose of this study was to investigate some problems that are of importance for the technical evaluation of the densification effect in granular soil. These problems include the pounder efficiency and the dynamic responses of pounder and pore water pressure. It is hoped that the information from this study may be useful in the evaluation of effect of dynamic compaction and for future development.

2. SOIL CONDITIONS

The test site is at the Changi East in Singapore, where a reclamation project is being carried out for the future expansion of Changi Airport. Site exploration revealed that the subsoil consists of an upper hydraulic sandfill of 8 to 12m in thickness. The sandfill is underlain by marine clay of the Kallang formation, comprising soft to firm silty clay and sands of late Pleistocene and recent deposits. The marine member is generally separated by stiff reddish silty clays and peaty clays, which were created by exposure of the seabed to the atmosphere during the rise and fall of the sea level in the geological past. The marine clay is underlain by the old alluvium of cemented silty and clayey sand.

The site was reclaimed by hydraulic method using cutter suction dredgers with 15,000 to 20,000 HP. The pumped sandfill material was discharged through the pipe lines of 3 to 5 km long. The in-situ properties of the sandfill in test area were determined by the cone penetration tests (CPT). The CPT showed that hydraulically placed fill is likely to be 5 to 10 MPa above water table and 3 to 5 MPa below the water table.

Laboratory tests were conducted to investigate the properties of the hydraulic sandfill. The specific gravity of the sand determined using the procedures based on BS1377 (1990) is 2.68. Sieve analysis was carried out and the particle size distribution is shown in Fig. 1. The coefficient of uniformity ranges from 3 to 4, the mean grain size (D_{50}) ranges from 0.5 and 0.7, and the particle size ranges from 0.05 to 3.1 mm.

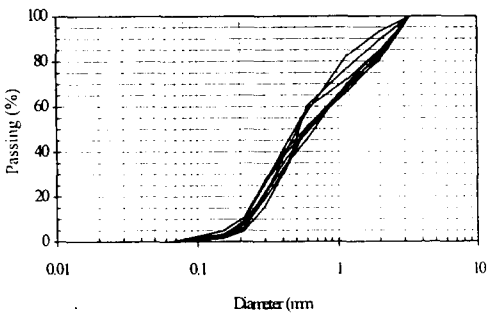

Fig. 1 Particle size distribution of sands at testing area

3. FIELD INSTRUMENTATION

An area of about 200 hectares is being compacted by dynamic compaction (DC), vibroflotation and Muller Resonance Compaction (MRC) at Changi Phase 1B, details of which was discussed by Choa et. al. (1997). During the compaction, the dynamic measurement for DC was carried out to understand the mechanisms of soil densification and the effectiveness of dynamic compaction at a trial location within the site. The pounder was made of three octagonal steel plates bolted together

with eight numbers of threaded bolts of 320mm in diameter. The nuts of 450mm in diameter are protruded from the base of the pounder, forming 200mm long legs. The weight of whole pounder is about 18 tons with 6.0 m2 base area.

Loster GmbH, Germany developed the dynamic measurement system. Sensors with different kinds of electrical interface such as piezoelectric type accelerometers and slot filter type piezometers send their signal to preamplifiers with changeable gain from 1 to 500 in compact acquisition boxes. The signals are transmitted to the central data acquisition system. The data acquisition system consists of 16 channels extendable to 32 channels and a notebook computer that is equipped with PCMCIA cards for data acquisition in sample frequency of maximum 320 kHz and conversion from analogue to digital.

The decelerations and the velocities of the pounder were measured by employing an accelerometer and two infrared beams that are intercepted by the dropping pounder immediately prior to the impact respectively. For this, a piezoelectric accelerometer was mounted on top of pounder and two sets of source and receiver for the infrared beams were installed 0.3m and 1.3m above ground surface at both sides of print point, which were facing each other in parallel. The change in pore water pressure was also measured by using slot filter type piezometers.

Seven single points were compacted with increasing drop heights of 3, 7, 10, 15 and 20 meters, and 20 drops were applied to every single point. The test was also performed with square grid of various spacing and different numbers of drops.

The dynamic measurement was carried out on all single points as well as a square grid of spacing of 5.0 meters in which pore water pressure was also measured. The crater depths and an array of benchmarks on the ground were surveyed to measure settlement under the pounder and ground movement around the pounder at every drop.

4. RESULTS OF FIELD MEASUREMENTS

From the measurements as mentioned earlier, the following evaluations were performed: (1) pounder impact, (2) pore water pressure response and (3) impact velocity.

4.1 Pounder Impact

The pounder acceleration was monitored by a vertical accelerometer mounted on top of the pounder. A typical result for the first drop in the time-domain is shown in Fig. 2(a). By integration of the deceleration signal with respect to impact time, the vibration velocity can be calculated using following equation (1),

$$v_{t=} \int a_t \, dt + C_t \qquad (1)$$

where C_v was integration constant. By assuming that the impact velocity is zero at the end of main deceleration signals, the integration constant can be calculated, which allows the correction for zero-shift after integration. In Fig. 2(b), the theoretically calculated impact velocity is also shown as a horizontal line, which makes it possible to estimate the energy loss during the release of the pounder. The velocity measured by photosensors of GT7SN (discussed later) is also shown in Fig. 2(b) for the comparison. The calculated velocity is found to be in good agreement with the measured velocity.

By integration of the calculated velocity, the displacement of pounder can be estimated using

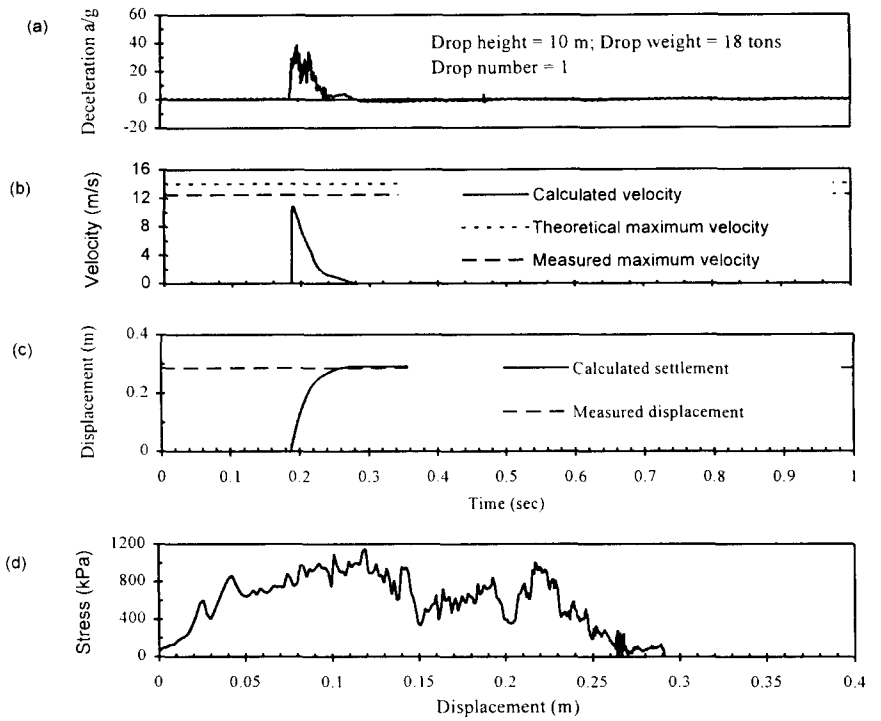

Fig. 2 Pounder response to drop number of 1: (a) deceleration measured on the pounder; (b) velocity determined from deceleration signal; (c) displacement determ from deceleration signal; (d) impact stress-displacement curve on ground surface

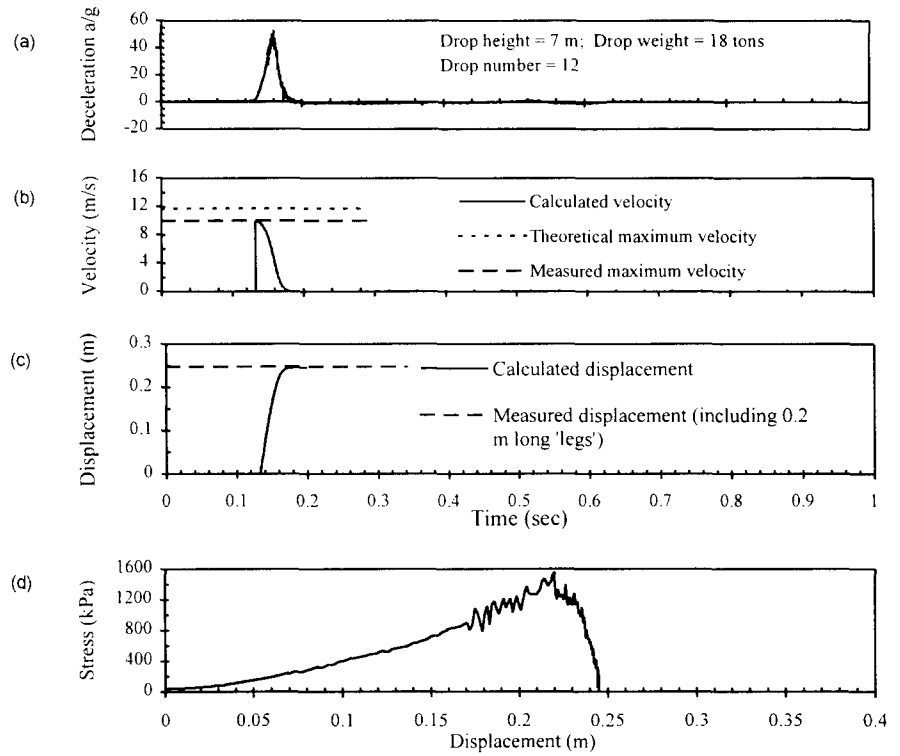

Fig. 3 Pounder response to drop number of 12: (a) deceleration measured on the pounder; (b) velocity determined from deceleration signal; (c) displacement determ from deceleration signal; (d) impact stress-displacement curve on ground surface

following equation (2),

$$d_t = \int v_t dt + C_a \qquad (2)$$

as shown in (Fig. 2(c)), where C_d was determined based on the actual at rest incremental pounder displacement for a particular drop. The calculated displacement is found to be similar to the manually measured value. From the measured pounder deceleration and the calculated displacement, an impact stress-displacement curve can be established as shown in Fig. 2(d). A typical result of decelerations recorded after the 6th drop is shown in Fig. 3, which is different from the first drop in the impact stress behavior. Before reaching maximum impact stress, the slope of loading portion of impact stress-displacement curve (Fig. 3(d)) is smoother than that of 1st drop (Fig. 2(d)). It was observed during the tests that the sand within a depth of about 0.3m from the bottom of crater was very loose due to the disturbance with successive drop, which resulted from the slippage of sands into the crater when the pounder was removed from the crater, and the 0.2m long legs protruded from the base of the pounder punching through this layer. Thus the displacement calculated from the deceleration records should be considered inclusive of 0.2m long plate extensions. Considering this factor, the calculated displacement is in good agreement with manually measured displacement as shown in Fig. 4.

In this study, the main part of deceleration signals is used for the calculation of impact velocity and displacement. When the impact velocity and displacement are determined by assuming the impact velocity to be zero at the end of main part of deceleration signals, these are not so sensitive to the deceleration zero line, which is usually not well known. But the unloading phase in the stress-displacement curve may not indicate a typical stress-stain behavior of sand. As shown in Figs. 2(d) and 3(d), the displacements still increase as the dynamic stress unloads, which contradicts the stress-strain behavior of sand. The deceleration records over relatively long periods after the main part of deceleration signals must be considered in the integration range for the accurate determination of sand behavior during the unloading phase. However the deceleration records after main part of deceleration is very sensitive to deceleration zero line since small measurement errors made over relatively long periods of time are summed up. A small shift of the deceleration zero level may lead to a significant error in the calculation of velocity and displacement. Thus the use of main part of deceleration records may provide a reasonable estimation of pounder velocity and displacement but could not give a correct indicator of sand behavior during the unloading phase.

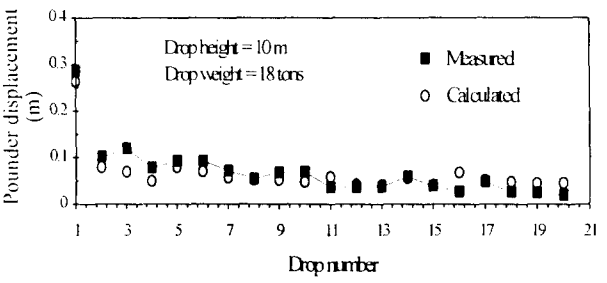

Fig. 4 Comparison of calculated and manually measured displacement of each drop for a seres of tests

To study the changes in deceleration or impact stress with respect to the number of drop, a series of the deceleration records of the pounder are shown in Fig. 5 and the changes in peak deceleration with drop number are shown in Fig. 6. In the first few drops, the peak deceleration signals increase with the numbers of drops and the deceleration duration becomes short which means the sand under pounder was getting denser. This also indicated the first few drops induce punching shear and compaction displacement in the relatively dense surface soils as the momentum of the dropping pounder decays. After a few drops, the peak decelerations become smaller and constant. This indicates that the sand under the pounder became loose due to the 0.2m long legs

protruded from the base of the pounder and the changed crater shape. When the pounder was

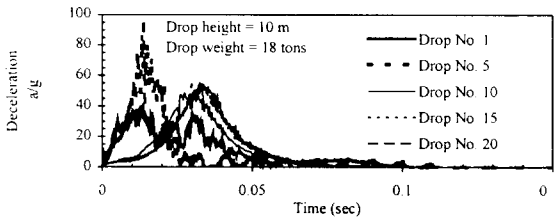

Fig. 5 Typical deceleration records

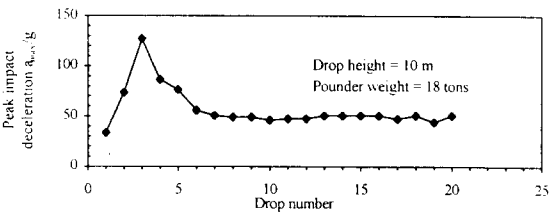

Fig. 6 A typical relationship between peak impact deceleration and drop number

removed from the crater, loose sand slipped down to the crater edge, and created smoother slopes in crater. The loose sand situated at the bottom of the crater and legs of the pounder affected successive measured deceleration. Therefore the dynamic modulus determined from the slope of stress-displacement curve indicates the sand behavior of the disturbed zone near the bottom of pounder and does not reflect the sand compaction behavior under the disturbed zone. The sand under disturbed zone becomes dense with the increase of number of drops, which could not be reflected by the measured deceleration. Other in-situ tests such as cone penetration test must be used to determine sand densification. This finding contradicts the results of the laboratory model tests suggested by Heh (1991). In the laboratory model tests, the pounders used in the model tests were much smaller than that used at field and consequently the size of craters created by smaller pounder was much smaller. It may be possible to minimize the effect of the change in crater shape in the model tests. Then the deceleration measurements at the laboratory may reflect the sand compaction behavior under dynamic compaction since the peak deceleration increases with the number of drops. However the laboratory model tests could not indicate the relationship of the loss of input energies and drop number. Thus it must be taken into consideration for the application of the results from laboratory model tests to the field.

4.2 Pore Water Pressure Response

Two piezometers were installed at depth of about 5m with different distances along the diagonal line as shown in Fig. 7. The change in pore water pressure was recorded during every impact of the pounder in this particular square grid. A sequence of compaction in this grid was that at 10 drops from 20m height were applied to every print point in numerical order. A typical signal of the variation of induced pore water pressure due to the impact during pounding at 1 is shown in Fig. 8.

It can be seen that the response of pore water pressure decrease with respect to distance. It was observed that the residual pore water pressure after the peak was dissipated for a period of 2 to 3 minutes in all cases. The maximum change in pore water pressure of the piezometer No.2 (p2) installed in near center of the square grid is presented with respect to number of drops in Fig. 9(a). The result indicates that the higher pore water pressure was generated as the surrounding soil of the piezometer tip was densified. Fig. 10 shows one of the results from the pore pressure measurement during pounding at 2. It is interesting to note that the peak pore water pressures p1 are higher than those of p2, even though p1 was situated further than p2 from pounding point. This is probably due to the reason that the structure of surrounding soil of p2 was likely to be destroyed during the pounding at 2, which caused a higher permeability and less peak pore water pressure

induced due to the impact. This should be verified with modeling test. Fig.9(b) shows induced pore water pressure p1 with respect to the number of drops for different distances from pounding point. It could be realized that a variation of pore water pressure is not much within a short distance which means that stress peak distributed around pounding point is almost the same within the limited zone with shape of a pressure bulb or perhaps a truncated cone. Fig. 9(c) shows the results of pore water pressure measurement obtained from p1 and p2 during pounding at 3 and 4. It could be noted that the similar peak pore water pressures were induced when the pore pressuremeters were installed at the same distance from pounding point however less peak pore water pressures are generated when the surrounding soil is less densified, even though the pore pressuremeters are installed at the same distance.

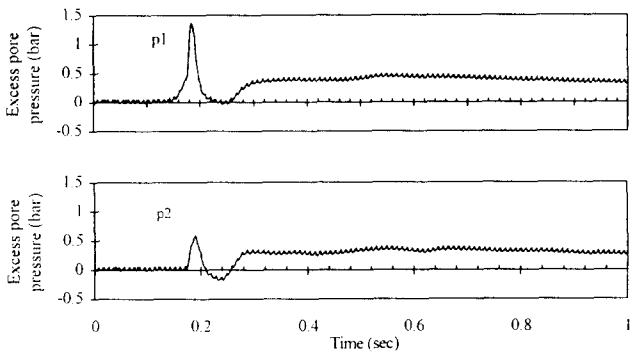

Fig. 8 Response of excess pore pressure during pounding at drop location 1

4.3 Impact Velocities

Photosensors of GT7SN with built in amplifier that was designed to detect an object, were used to measure the velocity of pounder immediately prior to impact. This device consists of a timer and two pairs of transmitters and receivers for infrared beams with an object resolution of 6mm. Two pairs were installed 0.3m and 1.3m above ground surface respectively at both sides of the

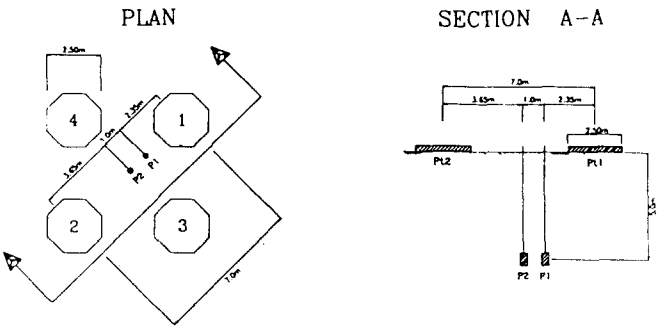

Fig. 7 Layout of piezometer installation

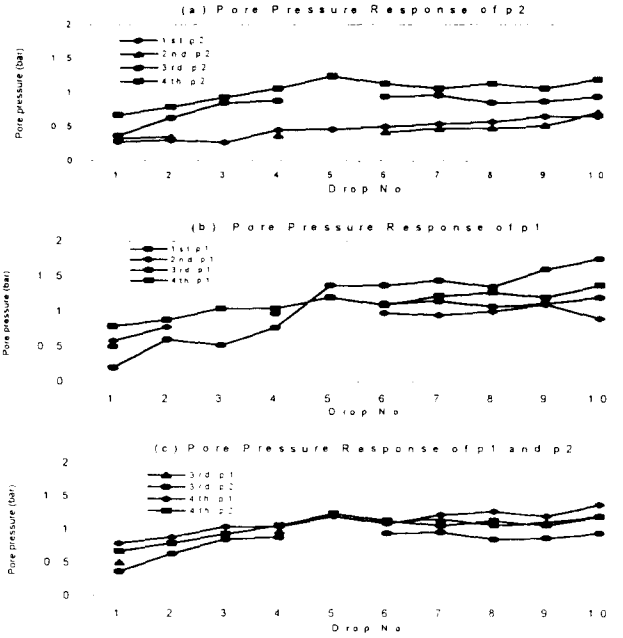

Fig. 9 Response of excess pore pressure with drop numbers

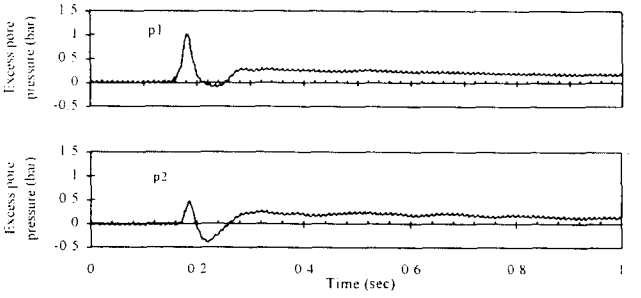

Fig. 10 Response of excess pore pressure during pounding at drop location 2

pounding point and each pair was facing each other in parallel, the first one of which is acting as start mode and the second one as stop mode when the pounder crossed these infrared beams. The times taken for the pounder to cross two beams were measured, which could be converted to the impact velocity.

Unfortunately the timer could be readable with two decimals which caused a significant error in the calculation of impact velocity. The ratios of measured impact velocities to theoretical impact velocities for a free falling pounder without air resistance are compared with respect to the drop heights in Table 1. It can be seen from this measurement that the ratio of measured to theoretical velocity is about 85 % with an error range of 3 to 7.8 %. The reduction in impact velocity is probably due to air resistance and friction losses in the winch system i.e. friction losses between cable and cable drum during unwinding.

Table 1 Ratios of measured to theoretical impact maximum velocities

Drop Height (m)	Measured Time (sec)	Impact Velocity (m/sec^2)		Ratio (%) (1)/(2)
		Measured (1)	Theoretical (2)	
3.0	0.15	6.7	7.67	87
7.0	0.10	10.0	11.71	85
10.0	0.08	12.5	14.00	89
15.0	0.07	14.3	17.50	83
20.0	0.06	16.6	19.80	84

5. CONCLUSIONS

In this experimental study on the dynamic measurement of dynamic compaction, the following conclusion can be made:

(1) The deceleration measurements on the pounder can provide reasonable estimations of the pounder velocity and displacement, if the main part of deceleration records are used for calculation.

(2) The dynamic stress and modulus derived from the deceleration records cannot reflect the sand behavior during the field dynamic compaction.

(3) The value of excess pore pressure generated by the dynamic compaction depends on the density of sand. The higher excess pore pressure was generated in denser sand.

(4) The maximum impact velocity is about 85% of theoretical maximum velocity.

REFERENCES

Choa V., Bo, M. W., Arulrajah, A. and Na, Y. M. (1997): Overview of Densification of Granular Soil by Deep Compaction Methods, International Conference on Ground Improvement Techniques, Macau, 131-140.

Heh King-Sen (1991): Dynamic Compaction of Sand, Ph. D. thesis, Polytechnic University, Michigan, U. S. A.

Mayne, P. W., Jones, J. S. and Dumas, J. C. (1984): Ground Response to Dynamic Compaction, Journal of Geotechnical Engineering Division, ASCE, Vol. 110, No. 6, 757-774.